Parallel Mechanisms in Acetylcholinesterase-Catalyzed Hydrolysis of Choline Esters

Trevor Selwood, Shawn R. Feaster, Michael J. States, Alton N. Pryor, and Daniel M. Quinn*

Contribution from the Department of Chemistry, The University of Iowa, Iowa City, Iowa 52242

Received November 4, 1992®

Abstract: The mechanisms of acetylcholinesterase (AChE)-catalyzed hydrolyses of four choline esters, (acetylthio)-choline, (propanoylthio)choline, (butanoylthio)choline, and benzoylcholine, have been compared by measuring relative activities and pH–rate effects. The reactivity of *Electrophorus electricus* AChE toward these substrates decreases in the above order and spans a 1500-fold range of k_{cat} and a 2300-fold range of k_{cat}/K_m. The pH–V/K profile for (acetylthio)choline hydrolysis shows that activity depends on the basic form of an active site residue, probably H440, that has a $pK_a = 6.22 \pm 0.03$ (Rao, M.; *et al. J. Am. Chem. Soc.* **1993**, *115*, in press; ref 23). The pH–V/K profile for (propanoylthio)choline shows similar behavior and gives a $pK_a = 6.42 \pm 0.03$. The pH–V/K profile for (butanoylthio)-choline hydrolysis, on the other hand, shows that activity depends on the basic forms of three active site residues, two that have pK_a values of 4.72 ± 0.02 and one that has a pK_a value of 6.3 ± 0.1. For the least reactive substrate, benzoylcholine, pH–V and pH–V/K profiles depend only on the ionizations of the residues that have the lower pK_a values, 4.77 ± 0.03 and 4.71 ± 0.03, respectively. The solvent isotope effects for benzoylcholine hydrolysis are $^DV/K = 1.91 \pm 0.06$ and $^DV = 1.7 \pm 0.3$, and proton inventories of these parameters suggest that a carboxylate residue functions as a general base catalyst. *Torpedo californica* AChE also displays a high kinetic discrimination for (acetylthio)-choline versus (butanoylthio)choline; the ratio of k_{cat} values for the respective substrates is 3800, while the corresponding k_{cat}/K_m ratio is 850. The pH–V/K profile for hydrolysis of (acetylthio)choline depends on a single residue that has $pK_a = 6.33 \pm 0.03$, while that for hydrolysis of (butanoylthio)choline has a maximum at pH ~5.5 and depends on amino acid residues that have pK_a values of 4.99 ± 0.07 and 6.1 ± 0.3. Therefore, parallel mechanisms operate in acetylcholinesterase-catalyzed hydrolysis of choline esters. The biomimetic substrate (acetylthio)choline and the homologue (propanoylthio)choline are hydrolyzed via nucleophilic and general acid–base catalysis by the active site triad S200–H440–E327. As the substrate reactivity decreases, the mechanism shifts progressively from triad catalysis to one that likely involves general base catalysis by E199 of direct water attack on the scissile carbonyl. Molecular modeling suggests that the sterically circumscribed acyl-binding site accommodates the acetyl and propanoyl functions of choline substrates. However, the sterically encumbered butanoyl and benzoyl functions are less well accommodated in the acyl-binding site, and thus the corresponding substrates apparently occupy an alternate binding site in the active site gorge from which catalysis by E199 is effected.

Acetylcholinesterase (AChE[1]) catalyzes the hydrolysis of the neurotransmitter acetylcholine (ACh) at nerve–nerve and neuromuscular junctions.[2-5] The enzyme effects this task with high efficiency. Consider the kinetic mechanism for ACh turnover (Scheme I) and the corresponding expression for V/K:

$$V/K = k_{cat}[E]_T/K_m = \frac{k_1 k_3 [E]_T}{k_2 + k_3} \quad (1)$$

P and Q are the respective choline and acetate products. Equation 1 shows that k_{cat}/K_m (and hence V/K) monitors events that convert free enzyme and free substrate ($E + A$) to the acylenzyme intermediate F. The effects of ionic strength[6] and solvent viscosity[7] on k_{cat}/K_m of AChE-catalyzed hydrolysis of (acetylthio)choline (ATCh) indicate that acylation is rate limited by diffusional encounter of substrate and enzyme, i.e. $k_{cat}/K_m = k_1$. ATCh is a close biomimic of ACh,[2,8] which suggests that the ACh reaction is also diffusion controlled. Therefore, AChE operates at the speed limit of biological catalysis.[9]

Scheme I

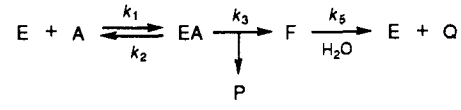

Unfortunately, the considerable catalytic power of AChE toward ACh and ATCh masks the transition state of the chemical step in the acylation stage of catalysis (represented by k_3 in Scheme I) from characterization by such probes as kinetic isotope effects. A time-honored method for overcoming this problem is to utilize alternate substrates whose reactivities are lower than that of the physiological substrate. Usually this lowered reactivity is accompanied by partial or complete exposure of the chemical transition state as rate limiting. With this is mind we undertook

* Author to whom correspondence should be addressed.

® Abstract published in *Advance ACS Abstracts*, October 1, 1993.

(1) Abbreviations: ACh, acetylcholine; AChE, acetylcholinesterase; ATCh, (acetylthio)choline; BuTCh, (butanoylthio)choline; BzCh, benzoylcholine; DTNB, 5,5′-dithiobis(2-nitrobenzoic acid); EE-AChE, *Electrophorus electricus* AChE; TC-AChE, *Torpedo californica* AChE; MES, 2-(*N*-morpholino)ethanesulfonic acid; PrTCh, (propanoylthio)choline; K, the Michaelis constant K_m; V, the maximal velocity V_{max}; V/K, V_{max}/K_m; $^DV = V^{H_2O}/V^{D_2O}$, solvent isotope effect on V; $^DV/K = (V/K)^{H_2O}/(V/K)^{D_2O}$, solvent isotope effect on V/K. Single letter amino acid codes: E, glutamate; H, histidine; S, serine.

(2) Quinn, D. M. *Chem. Rev.* **1987**, *87*, 955–979.

(3) Rosenberry, T. L. *Adv. Enzymol. Relat. Areas Mol. Biol.* **1975**, *43*, 103–218.

(4) Taylor, P. In *Pharmacological Basis of Therapeutics*; Gilman, A. G., Goodman, L. S., Murad, F., Eds.; MacMillan: New York, 1985; pp 110–129.

(5) Froede, H. C.; Wilson, I. B. In *The Enzymes*, 3rd ed.; Boyer, P. D., Ed.; Academic: New York, 1971; Vol. 5, pp 87–114.

(6) Nolte, H.-J.; Rosenberry, T. L.; Neumann, E. *Biochemistry* **1980**, *19*, 3705–3711.

(7) Bazelyansky, M.; Robey, E.; Kirsch, J. F. *Biochemistry* **1986**, *25*, 125–130.

(8) Froede, H. C.; Wilson, I. B. *J. Biol. Chem.* **1984**, *259*, 11010–11013.

(9) Quinn, D. M.; Pryor, A. N.; Selwood, T.; Lee, B.-H.; Acheson, S. A.; Barlow, P. N. In *Cholinesterases: Structure, Function, Mechanism, Genetics, and Cell Biology*; Massoulié, J., Bacou, F., Barnard, E., Chatonnet, A., Doctor, B. P., Quinn, D. M., Eds.; American Chemical Society: Washington, DC, 1991; pp 252–257.

0002-7863/93/1515-10477$04.00/0

to characterize the transition state of the k_3 step by measuring solvent isotope and pH–rate effects with choline substrates that span a wide reactivity range. As shall be seen herein, this well-intentioned but misguided approach led to the discovery of parallel reaction pathways for AChE-catalyzed hydrolysis of choline esters.[10]

Experimental Section

Materials. EE-AChE (EC 3.1.1.7), grade V-S lyophilized powder, was purchased from Sigma Chemical Co. and prior to use was dissolved in 0.05 M sodium phosphate buffer (ionic strength = 0.2 with added NaCl), pH 6.8 or 7.3. TC-AChE was purified as described by Sussman *et al.*[11] The active site concentrations of AChE preparations were determined by fluorescent titration with diethyl umbelliferyl phosphate.[12] PrTCh iodide was purchased from Aldrich Chemical Co. ATCh chloride, BuTCh iodide, BzCh chloride, DTNB, $NaH_2PO_4 \cdot H_2O$, $Na_2HPO_4 \cdot 7H_2O$, MES, sodium acetate, and diethyl *p*-nitrophenyl phosphate were used as received from Sigma Chemical Co. Water was distilled and deionized by passage through a Barnstead D8922 mixed-bed ion-exchange column (Sybron Corp.). Deuterium oxide (99.8% D) was purchased from Aldrich Chemical Co. and used as received. NaCl was used as received from EM Science. Aqueous 0.1 N NaOH was purchased from Fisher Scientific.

Enzyme Kinetics and Data Treatment. AChE-catalyzed hydrolysis of thiocholine esters was monitored by following the production of thiocholine at 412 nm by the coupled DTNB assay described by Ellman *et al.*[13] Time courses for AChE-catalyzed hydrolysis of BzCh were followed at 240 nm ($[A]_0 < K_m/2$), 250 nm ($K_m/2 < [A]_0 < K_m$), or 288 nm ($[A]_0 > K_m$). Assays were conducted on Beckman DU40 or HP8452A UV–visible spectrophotometers whose cell compartments were thermostated by using refrigerated, circulating water baths. The Michaelis–Menten parameters V and K and the pseudo-first-order rate constant V/K were determined as described previously.[14a] Nonenzymic substrate turnover was determined by measuring rates under the same conditions as those of AChE assays, but in the absence of enzyme. Consequently, rates in the presence of AChE have been corrected to account for nonenzymic hydrolysis.

Buffer pH values were measured on a Corning model 125 pH meter that is equipped with a glass combination electrode; 0.4 was added to the pH meter reading to determine pD values of D_2O buffers.[15] Solvent isotope effects were determined by measuring rates in equivalently buffered solutions of H_2O and D_2O.[16] Proton inventories were determined by measuring rates in various volumetric mixtures of equivalent isotopic buffers. The theory and practice of solvent isotope effect and proton inventory experiments have been extensively reviewed.[16] Buffer compositions and other reaction conditions are specified in figure legends and table footnotes. Particular computational methods for analyzing pH–rate profiles and proton inventories are described at appropriate locations in the Results.

AChE Inhibition. Two types of inhibition experiments were conducted to show that fast and slow choline substrates are hydrolyzed at overlapping sites on AChE. In the first experiment 180 nM AChE was incubated with 0.05 mM diethyl *p*-nitrophenyl phosphate at 25.0 ± 0.2 °C in 0.1 M sodium phosphate buffer, pH 7.36, that contained 0.1 N NaCl. At various times aliquots of this solution were removed and initial velocities were measured in the same buffer for hydrolysis of 0.5 mM ATCh or 0.2 mM BzCh. In the second experiment, time courses for AChE-catalyzed hydrolysis of ATCh were measured at 25.0 ± 0.1 °C in 0.05 M sodium phosphate buffer, pH 7.3 (μ = 0.2 with NaCl), that contained different fixed concentrations of BzCh. The time courses were fit to the integrated Michaelis–Menten equation, and the pattern of inhibition was examined by constructing Lineweaver–Burk plots,[17] as described in the Results.

Base-Catalyzed Hydrolysis of BzCh. First-order rate constants for HO^--catalyzed hydrolysis of BzCh were determined as a function of $[HO^-]$. Reactions were conducted at 25.1 ± 0.1 °C in 1.01 mL of aqueous sodium hydroxide that contained 0.063 mM BzCh, 1.0–100 mM HO^-, and sufficient NaCl to give μ = 0.1, and were monitored at 288 nm for at least three half-lives.

Molecular Modeling. The Sybyl molecular modeling and graphics program (Tripos Associates, St. Louis, MO) was used on Silicon Graphics workstations of the University of Iowa Image Analysis Facility to construct models for tetrahedral intermediates in the acylation stage of AChE-catalyzed hydrolysis of ATCh and BuTCh. The atomic coordinates of the crystal structure of *Torpedo californica* AChE[18] were kindly provided by Professor Joel Sussman of the Weizmann Institute, Rehovot, Israel. The modeling process consisted of the following steps: (a) water molecules were removed from the structure, (b) the structural elements of the substrate were constructed and attached to the γ-oxygen of S200, and (c) the structure of the complex was optimized by molecular mechanics, using the Tripos force field[19] of the Sybyl program. The substrate-derived portion of the complex and all amino acid side chains within 10 Å thereof were allowed to move; the atomic positions of the peptide backbone and all other amino acid side chains were constrained. Lone pairs, hydrogen atoms, and electrostatics[20,21] were included in the molecular mechanics calculations.

Results

Comparison of Rate Constants for Choline Ester Substrates. V and K for EE-AChE-catalyzed hydrolysis of BzCh were measured and the corresponding values of k_{cat} and k_{cat}/K_m calculated. These results are displayed in Table I and compared therein to published values[14a] for EE-AChE-catalyzed hydrolysis of ATCh, PrTCh, and BuTCh. The activity trend for both k_{cat} and k_{cat}/K_m is ATCh > PrTCh ≫ BuTCh > BzCh; the ranges of the respective rate constants are 1500- and 2300-fold. Despite the much decreased reactivity of BzCh versus ATCh, AChE is a potent catalyst of BzCh hydrolysis. This fact is demonstrated by comparing rate constants for EE-AChE-catalyzed and HO^--catalyzed hydrolyses of BzCh. The dependence of the observed first-order rate constant on $[HO^-]$ for BzCh hydrolysis was observed to be linear and is given by the following equation:

(10) (a) A preliminary account of some of the results described in this paper was presented at the 36th OHOLO Conference in Eilat, Israel, April 6–10, 1992: Quinn, D. M.; Selwood, T.; Pryor, A. N.; Lee, B. H.; Leu, L.-S.; Acheson, S. A.; Silman, I.; Doctor, B. P.; Rosenberry, T. L. In *Multidisciplinary Approaches to Cholinesterase Functions*; Shafferman, A., Velan, B., Eds.; Plenum: New York, 1992; pp 141–148. (b) Erjdan Salih has evaluated the pH-rate behavior of the AChE turnover of a wide range of substrates and proposes that catalysis occurs in two protonic states of the enzyme. This is, in effect, a demonstration of parallel pathways for AChE catalysis and thus supports the AChE mechanistic diversity reported herein. See: Salih, E. *Biochem. J.* **1992**, *285*, 451–460.

(11) Sussman, J. L.; Harel, M.; Frolow, F.; Varon, L.; Toker, L.; Futerman, A. H.; Silman, I. *J. Mol. Biol.* **1988**, *203*, 821–823.

(12) Schlom, P. S.; Seravalli, J.; Gillespie, S.; Selwood, T.; Knuth, T. M.; Nair, H. K.; Nyanda, A. M.; Doctor, B. P.; Quinn, D. M. *Chem. Res. Toxicol.*, submitted for publication.

(13) Ellman, G. L.; Courtney, K. D.; Andres, V., Jr.; Featherstone, R. M. *Biochem. Pharmacol.* **1961**, *7*, 88–95.

(14) (a) Pryor, A. N.; Selwood, T.; Leu, L.-S.; Andracki, M. A.; Lee, B. H.; Rao, M.; Rosenberry, T.; Doctor, B. P.; Silman, I.; Quinn, D. M. *J. Am. Chem. Soc.* **1992**, *114*, 3896–3900. (b) Radic, Z.; Gibney, G.; Kawamoto, S.; MacPhee-Quigley, K.; Bongiorno, C.; Taylor, P. *Biochemistry* **1992**, *31*, 9760–9767. (c) Vellom, D. C.; Radic, Z.; Li, Y.; Pickering, N. A.; Camp, S.; Taylor, P. *Biochemistry* **1993**, *32*, 12–17.

(15) Salomaa, P.; Schaleger, L. L.; Long, F. A. *J. Am. Chem. Soc.* **1964**, *86*, 1–7.

(16) (a) Schowen, K. B. J. In *Transition States of Biochemical Processes*; Gandour, R. D., Schowen, R. L., Eds.; Plenum: New York, 1978; pp 225–283. (b) Schowen, K. B.; Schowen, R. L. *Methods Enzymol.* **1982**, *87*, 551–606. (c) Venkatasubban, K. S.; Schowen, R. L. *CRC Crit. Rev. Biochem.* **1985**, *17*, 1–44. (d) Quinn, D. M.; Sutton, L. D. In *Enzyme Mechanism from Isotope Effects*; Cook, P. F., Ed.; CRC Press: Boca Raton, FL, 1991; pp 73–126.

(17) Stout, J. S.; Sutton, L. D.; Quinn, D. M. *Biochim. Biophys. Acta* **1985**, *837*, 6–12.

(18) Sussman, J. L.; Harel, M.; Frolow, F.; Oefner, C.; Goldman, A.; Toker, L.; Silman, I. *Science* **1991**, *253*, 872–879.

(19) (a) Clark, M.; Cramer, R. D., III; Van Opdenbosch, N. *J. Comput. Chem.* **1989**, *10*, 982–1012. (b) White, D. N. J. *Comput. Chem.* **1977**, *1*, 225–233. (c) Vinter, J. G.; Davis, A.; Saunders, M. R. *J. Comput.-Aided Mol. Des.* **1987**, *1*, 31–51. (d) Motoc, I.; Dammkoehler, R. A.; Mayer, D.; Labanowski, I. *Quant. Struct.-Act. Relat.* **1986**, *5*, 99–105. (e) Labanowski, J.; Motoc, I.; Naylor, C. B.; Mayer, D.; Dammkoehler, R. A. *Quant. Struct.-Act. Relat.* **1986**, *5*, 138–152.

(20) Contributions to electrostatics from π electrons were calculated by the Hückel method: (a) Streitwieser, A. *Molecular Orbital Theory for Organic Chemists*; Wiley: New York, 1961; pp 3–145. (b) Purcel, W. P.; Singer, J. A. *J. Chem. Eng. Data* **1967**, *12*, 235–246.

(21) Contributions to electrostatics from σ electrons were calculated by the Gasteiger–Marsili method: (a) Gasteiger, J.; Marsili, M. *Tetrahedron* **1980**, *36*, 3219–3228. (b) Marsili, M.; Gasteiger, J. *Croat. Chem. Acta* **1980**, *53*, 601–614. (c) Gasteiger, J.; Marsili, M. *Org. Magn. Reson.* **1981**, *15*, 353–360.

Table I. Comparison of Michaelis–Menten Parameters for AChE-Catalyzed Hydrolysis of Choline Esters

enzyme	substrate	k_{cat} (s^{-1})	K_m (mM)	$10^{-4}(k_{cat}/K_m)$ (M^{-1} s^{-1})
EE-AChE	ATCh[a]	8800 ± 200	0.114 ± 0.009	7700 ± 600
	PrTCh[a]	3660 ± 70	0.15 ± 0.01	2500 ± 200
	BuTCh[a]	95 ± 3	1.2 ± 0.1	8.0 ± 0.7
	BzCh[b]	6.0 ± 0.7	0.18 ± 0.04	3.3 ± 0.8
				2.1 ± 0.2[c]
TC-AChE	ATCh[a]	4280 ± 60	0.063 ± 0.004	6800 ± 400
	BuTCh[d]	1.16 ± 0.05	0.015 ± 0.003	8 ± 2
		5.4 ± 0.5		

[a] Data are taken from ref 14a. [b] Reactions were run at pH 7.26 and 25.2 ± 0.1 °C in 0.1 M sodium phosphate buffer that contained 0.06 N NaCl (μ = 0.3), 120 nM AChE, and $[BzCh]_0$ = 0.0495–0.495 mM. [c] Determined by first-order kinetics at pH 6.10 and 25.00 ± 0.05 °C in 0.1 M MES buffer that contained 0.1 N NaCl (μ = 0.2), 130 nM AChE, and $[BzCh]_0$ = 52 μM (= K_m/7). [d] Reaction conditions are given in the legend of Figure 1.

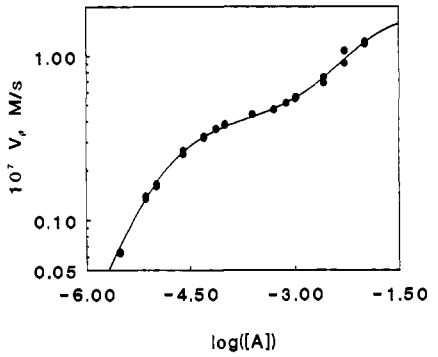

Figure 1. Dependence of initial velocity on substrate concentration for TC-AChE-catalyzed hydrolysis of BuTCh. Reactions were run at 25.2 ± 0.1 °C in 0.1 M sodium phosphate buffer, pH 7.85, that contained 0.011 N NaCl (μ = 0.3), 1.5 mM DTNB, 35 nM TC-AChE, and the indicated concentrations of BuTCh. The data were fit by nonlinear least-squares procedures[22] to eq 3, as described in the text, to give k_{cat} = 1.16 ± 0.05 s^{-1}, K_m = 0.015 ± 0.003 mM, β = 4.7 ± 0.4, and K_A = 9 ± 2 mM. The y axis is logarithmic and the independent variable is plotted as log([A]) to emphasize the two substrate binding interactions.

$$k_{obs} = (0.92 \pm 0.01\ M^{-1}\ s^{-1})[HO^-] - (6 \pm 8) \times 10^{-4}\ s^{-1} \quad (2)$$

Presumably the intercept arises from an H_2O-catalyzed pathway, but given its experimental uncertainty, further consideration of this term is neither wise nor warranted. The k_{cat} = 6 s^{-1} for BzCh hydrolysis in Table I was measured at pH 7.26, and thus $[HO^-]$ = 1.8 × 10^{-7} M. The corresponding pseudo-first-order rate constant for HO^- catalysis, calculated from the slope of eq 2, is 1.7 × 10^{-7} s^{-1}, and thus is 3.5 × 10^7-fold slower than k_{cat} for AChE catalysis.

TC-AChE-catalyzed hydrolysis of BuTCh is subject to substrate activation, as the initial velocity plot of Figure 1 demonstrates. The data in Figure 1 were fit to eq 3,[22] which is based

$$V_i = \frac{k_{cat}[E]_T[A]\{K_A + \beta[A]\}}{[A]^2 + K_A[A] + K_mK_A} \quad (3)$$

on the activation mechanism in Scheme II. The dependence of initial velocity on [A] follows Michaelis–Menten kinetics when $[A] \ll K_A$, as the fit in Figure 1 shows and as eq 3 predicts. This analysis gives values for k_{cat} and K_m of BuTCh hydrolysis that are compared in Table I to those for TC-AChE-catalyzed hydrolysis of ATCh.[14a] As the data in the table show, ratios of k_{cat} and k_{cat}/K_m for ATCh versus BuTCh are 3800 and 850, respectively. Therefore, the substrate specificities of EE-AChE and TC-AChE for acetyl and butanoyl substrates are similar.

(22) Wentworth, W. E. *J. Chem. Educ.* **1965**, *42*, 96–103.

Scheme II

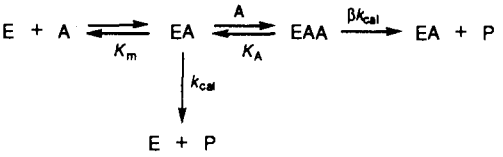

However, at higher substrate concentrations, binding of a second molecule of substrate to the enzyme (with a dissociation constant K_A = 9 ± 2 mM) stimulates k_{cat} of TC-AChE-catalyzed hydrolysis of BuTCh by a factor β = 4.7 ± 0.4.

pH–Rate Profiles. Decrease in reactivity for AChE-catalyzed hydrolysis of choline esters is accompanied by a systematic shift in the pH–rate behavior of the enzyme. The pH–V/K profile for EE-AChE-catalyzed hydrolysis of ATCh shows that activity depends on the basic form of a single active site amino acid side chain, likely that of H440, that has a pK_a = 6.22 ± 0.03.[23] For EE-AChE-catalyzed hydrolysis of PrTCh, the pH–V/K profile is also consistent with ionization of a single active site residue, as shown in Figure 2A. Nonlinear least-squares fitting[22] of the data in this figure to eq 4, which describes activity as depending on the basic form of a single ionizing residue, gives pK_a = 6.42 ± 0.03. The pH–V/K profile for TC-AChE-catalyzed hydrolysis of ATCh is similar in form, and yields a pK_a = 6.33 ± 0.02 (data not shown).

The pH–rate profiles for EE-AChE-catalyzed hydrolysis of BzCh bear no resemblance to that for ATCh or PrTCh, as the pH–V profile of Figure 2B shows. This profile was fit by nonlinear least-squares procedures[22] to each of the following two equations:

$$k = \frac{k_{lim}K_a}{K_a + [H^+]} \quad (4)$$

$$k = \frac{k_{lim}K_a^2}{K_a^2 + K_a[H^+] + [H^+]^2} \quad (5)$$

In these equations k is the observed rate or rate constant and k_{lim} is the corresponding least-squares calculated limiting value at high pH; K_a is the acid dissociation constant of the amino acid function on whose basic form activity depends. Equations 4 and 5, respectively, describe activity as depending on one and two titrable residues. The fit displayed in Figure 2B shows that the profile is well described by eq 5, and therefore that reactivity in EE-AChE-catalyzed hydrolysis of BzCh increases upon ionization of two residues that have pK_a values of 4.77 ± 0.03. The pH–V/K profile for BzCh hydrolysis previously reported by Quinn *et al.*[9] is also well described by ionization of two residues that have pK_a values of 4.71 ± 0.03. The similarity of the pH–V and pH–V/K profiles for BzCh hydrolysis suggests that the two rate constants monitor the same rate-limiting transition state, and the pK_a values suggest a role for carboxylate residues in the AChE active site.

BuTCh lies between ATCh and BzCh in reactivity, and the pH–V/K profile in Figure 3A for EE-AChE-catalyzed hydrolysis of BuTCh has characteristics of the pH-rate behaviors of both ATCh and BzCh, which were discussed above. The data in Figure 3A were fit to eq 6, which comes from the mechanism shown in

(23) Rao, M.; Barlow, P. N.; Pryor, A. N.; Paneth, P.; O'Leary, M. H.; Quinn, D. M. *J. Am. Chem. Soc.*, in press.

(24) The fit on the base limb can be improved by fitting the profile to the following equation:

$$k_E = \frac{K_{a1}^2(k_{E1}[H^+]^2 + k_{E2}K_{a2}^2)}{K_{a1}^2K_{a2}^2 + K_{a1}^2[H^+]^2 + [H^+]^4}$$

However, the resulting ionization constants are pK_{a1} = 4.99 ± 0.07 and pK_{a2} = 6.1 ± 0.3 and hence are indistinguishable from those determined by fitting the profile to eq 6.

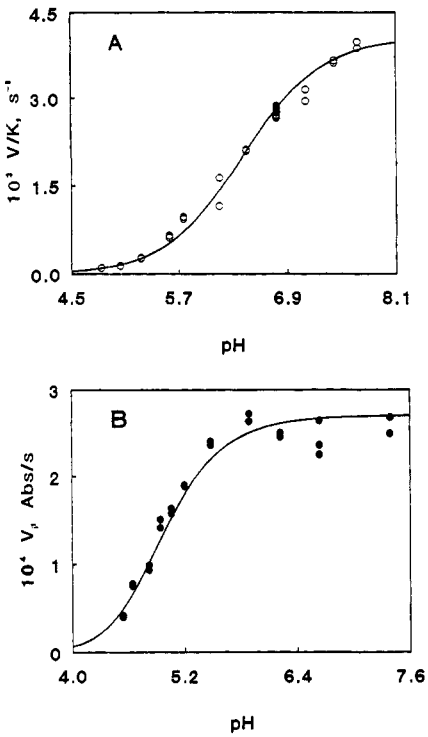

Figure 2. pH–Rate profiles for EE-AChE-catalyzed hydrolysis of choline esters. (A) pH–V/K profile for hydrolysis of PrTCh. V/K values were determined by first-order kinetics at 25.0 ± 0.1 °C in 0.05 M sodium phosphate buffers, pH 5.75–7.67, or 0.05 M sodium acetate buffers, pH 4.83–5.59, that contained $[PrTCH]_0$ = 0.02 mM, 0.3 mM DTNB, 67 pM EE-EChE, and sufficient NaCl to give μ = 0.2. The nonlinear fit resulted from least-squares analysis[22] of the data according to eq 4 and gives pK_a = 6.42 ± 0.03. (B) pH–V profile for hydrolysis of BzCh. V values were determined by measuring initial rates at 25.0 ± 0.1 °C in 0.096 M buffers that contained 14.9 nM AChE, 4.05 mM BzCh (≥20K_m), and sufficient NaCl to give μ = 0.2. The buffer used was CH_3CO_2Na/CH_3CO_2H (pH < 5.5), MES (5.5 < pH < 6.6), or Na_2HPO_4/NaH_2PO_4 (pH > 6.64). The nonlinear line is a least-squares fit[22] to eq 5 and gives pK_a = 4.77 ± 0.03.

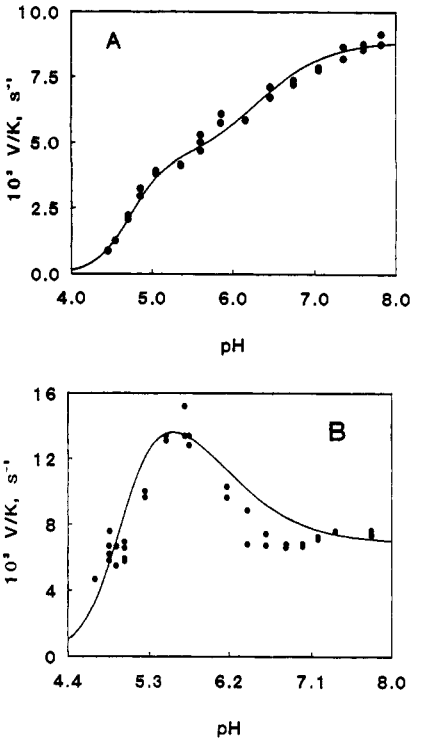

Figure 3. (A) pH–V/K profile for EE-AChE-catalyzed hydrolysis of BuTCh. V/K values were measured by first-order kinetics at 25.0 ± 0.1 °C in 0.05 M sodium acetate buffers, pH ≤ 5.6, or 0.05 M sodium phosphate buffers, pH > 5.6, that contained 110 nM AChE, 0.15 mM DTNB, $[BuTCh]_0$ = 0.058 mM (= K_m/20), and sufficient NaCl to give μ = 0.2. The nonlinear line is a least-squares fit[22] to eq 6, as described in the Results, and gives pK_a values of 4.72 ± 0.02 and 6.3 ± 0.1. (B) pH–V/K profile for TC-AChE-catalyzed hydrolysis of BuTCh. V/K values were determined by first-order kinetics at 25.24 ± 0.08 °C in 0.05 M sodium phosphate buffers, pH 5.75–7.77, or 0.05 M sodium acetate buffers, pH 4.69–5.70, that contained $[BuTCh]_0$ = 5.5 μM, 0.3 mM DTNB, 177 nM TC-AChE, and sufficient NaCl to give μ = 0.2. The nonlinear fit is a least-squares analysis[22] according to eq 6 and gives pK_a values of 5.02 ± 0.05 and 6.1 ± 0.2.

Scheme III. Parallel pathways for turnover of BuTCh are suggested in the scheme and make contributions k_{E1} and k_{E2} to k_{cat}/K_m. From the nonlinear-least-squares fit[22] to eq 6 shown

$$k_{cat}/K_m = \frac{K_{a1}^2\{k_{E1}[H^+] + k_{E2}K_{a2}\}}{K_{a1}^2\{[H^+] + K_{a2}\} + [H^+]^3} \qquad (6)$$

in Figure 3A the following constants were calculated: pK_{a1} = 4.72 ± 0.03, pK_{a2} = 6.3 ± 0.1, k_{E1} = (3.8 ± 0.2) × 10^4 M^{-1} s^{-1}, and k_{E2} = (8.1 ± 0.2) × 10^4 M^{-1} s^{-1}. Therefore, pK_{a1} is similar to the pK_a values determined from the pH-rate profiles for BzCh hydrolysis, while pK_{a2} is numerically similar to the pK_a values determined from the pH–V/K profiles for EE-AChE-catalyzed hydrolyses of ATCh[23] and PrTCh. The numerical similarity of k_{E1} and k_{E2} indicates that the parallel pathways make comparable contributions to AChE-catalyzed hydrolysis of BuTCh.

The pH–V/K profile for TC-AChE-catalyzed hydrolysis of BuTCh in Figure 3B provides a yet more dramatic indication of parallel reaction pathways. The profile has a maximum at pH 5.5–6 and levels off at high pH. Least-squares fitting[22] of the profile to eq 6 gives the following constants: pK_{a1} = 5.02 ± 0.05, pK_{a2} = 6.1 ± 0.2, k_{E1} = (9.4 ± 0.8) × 10^4 M^{-1} s^{-1}, and k_{E2} = (3.9 ± 0.3) × 10^4 M^{-1} s^{-1}.[24]

Solvent Isotope Effects. Values of V for EE-AChE-catalyzed hydrolysis of BzCh were determined in 0.1 M sodium phosphate buffers in H_2O and D_2O at pH 7.26 and pD 7.79, respectively. Values of V/K for BzCh hydrolysis were determined in 0.1 M MES buffers in H_2O and D_2O at pH 6.10 and pD 6.71,

Scheme III

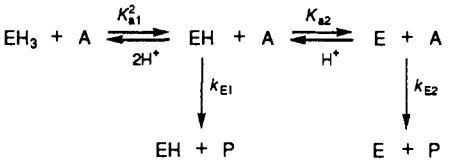

respectively. Additional reaction conditions for V and V/K measurements are respectively contained in footnotes b and c of Table I. The resulting kinetic solvent isotope effects are ^DV = 1.7 ± 0.3 and $^D(V/K)$ = 1.91 ± 0.06. The magnitudes of the isotope effects suggest that proton transfer is an element of transition-state stabilization.

Proton inventories of V and V/K were conducted to further elaborate transition-state protonic interactions for EE-AChE-catalyzed hydrolysis of BzCh. The proton inventory of V bulges upward, as displayed in Figure 4. The following equation is the general expression for proton inventories of rates or rate constants:[16]

$$k_n = k_0 \frac{\prod_i (1 - n + n\phi_i^T)}{\prod_i (1 - n + n\phi_i^R)} \qquad (7)$$

This equation shows that the dependence of k_n on n, the atom fraction of deuterium in solvent isotopic mixtures, contains a product of terms in the numerator and denominator for i transition-state and reactant-state protons that have respective fractionation

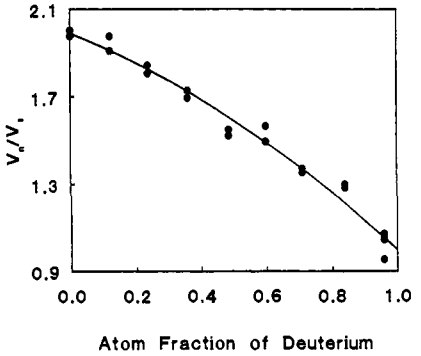

Figure 4. Proton inventory for V of EE-AChE-catalyzed hydrolysis of BzCh. V values were determined by measuring initial rates of BzCh hydrolysis at 25.23 ± 0.07 °C in 0.1 M MES buffers (pH 6.10 in H_2O, pD 6.71 in D_2O, and mixtures of these) that contained 0.1 N NaCl (μ = 0.15), [AChE] = 14.9 nM, and [BzCh] = 4.04 mM (= $22K_m$). Data are plotted as V_n/V_1, where V_1 is the least-squares extrapolated value of V for $n = 1$, and therefore the y-axis intercept is $V_0/V_1 = 1.99$, the solvent isotope effect. The nonlinear line is a least-squares fit[22] to eq 7 and gives $\phi^T = 0.36 \pm 0.03$ and $Z = 0.85 \pm 0.03$.

factors ϕ_i^T and ϕ_i^R that are $\neq 1$. The contribution of a transition-state proton transfer to the isotope effect is just $1/\phi^T$, while the contribution of a reactant-state proton is ϕ^R. The enzymic amino acid side chains that are typically involved in nucleophilic or general acid-base catalysis have ϕ^R values ~ 1 (the SH of cysteine is an exception), so that eq 7 usually simplifies to a polynomial function of n.[16] However, the bulging-upward shape of the plot in Figure 4 requires either that serial isotopically insensitive and isotopically sensitive steps contribute to rate limitation or that there are offsetting contributions to the isotope effect from transition-state and reactant-state protons. A particular model that incorporates offsetting transition-state and reactant-state contributions is embodied in eq 8.[16d] In this equation the term

$$k_n = k_0(1 - n + n\phi^T)Z^{-2n} \quad (8)$$

$1 - n + n\phi^T$ arises from the isotope effect (i.e. ${}^Dk = 1/\phi^T$) generated by a transition-state proton transfer from an H_2O nucleophile to an enzymic carboxylate, while Z^{-2n} represents a reactant-state effect for transfer of two carboxylate functions from H_2O to D_2O. The latter term is referred to as a medium effect. The nonlinear least-squares fit[22] in Figure 4 gives $\phi^T = 0.36 \pm 0.03$ and $Z = 0.85 \pm 0.03$. The observed solvent isotope effect of 1.99 thus arises from a proton transfer that generates an isotope effect of $1/\phi^T = 2.8$ that is partially offset by a medium effect $Z^2 = 0.72$ due to solvation of two amino acid residues in the EA complex. The proton inventory of V/K (plot not shown) gave similar results: $\phi^T = 0.44 \pm 0.04$, $Z = 0.91 \pm 0.04$. Like the similarity of the pH–V and pH–V/K profiles, the similarity of the V and V/K proton inventories suggests that the two rate constants are monitoring the same rate-limiting transition state.

Inhibition Experiments. An important consideration is whether ATCh and slower choline substrates, in particular BzCh, are hydrolyzed at overlapping sites on AChE. The effect of the irreversible inhibitor diethyl p-nitrophenyl phosphate on AChE-catalyzed hydrolyses of ATCh and BzCh indicates that this is so. On 5 min of incubation with the inhibitor under the conditions described in the Experimental Section, ~95% activity was lost for both substrates. Moreover, BzCh behaves as a mixed reversible inhibitor of AChE-catalyzed hydrolysis of ATCh. Time courses were followed for complete turnover of ATCh in the presence of various concentrations of BzCh. The time courses were fit to the integrated Michaelis–Menten equation by nonlinear–least-squares methods,[22] and linear transforms, akin to Lineweaver–Burk plots, were constructed as described previously.[17] The effects of BzCh on the slopes of these plots suggests that ATCh binding and BzCh binding to the free enzyme are mutually exclusive, and the inhibition constant calculated from a slope replot[25] is $K_i = 0.60 \pm 0.04$ mM, in reasonable agreement with the K_m value given in Table I for BzCh. These results and that of the irreversible inhibition by diethyl p-nitrophenyl phosphate indicate that ATCh and BzCh are hydrolyzed at sites on AChE that overlap.

Discussion

The results described in this paper are suprising, in that, as substrate reactivity decreases, two AChEs respond by a change in mechanism. Several observations suggest that the cryptic mechanism[10] that is unmasked by slowly reacting choline substrates involves general base catalysis of water attack on the carbonyl carbon of the scissile ester: (1) pH–rate profiles show a systematic shift from dependence of activity on the basic form of a residue that has a $pK_a = 6.2$–6.4 to catalysis by a residue or residues that has a $pK_a = 4.7$–5. The higher pK_a that operates for fast substrates such as ATCh and PrTCh is likely that for H440 of the active site S200–H440–E327 triad,[2,18] while the lower pK_a suggests the involvement of carboxylate residues in the cryptic mechanism. (2) The shape of the proton inventory in Figure 4 is consistent with a reactant-state contribution to the observed solvent isotope effect, described herein as arising from a medium effect $Z = 0.85$ on two amino acid residues. Medium effects are observed especially when ionic species are transferred from H_2O to D_2O and reflect isotopic fractionation at numerous sites in the waters that solvate the ions.[16] The medium effect Z determined from the proton inventory agrees well with that described by Kresge *et al.*,[26] $Z = 0.89$, for transfer of $CH_3CO_2^-$ from H_2O to D_2O. (3) The Z value determined from the proton inventory agrees well with Z values of 0.76 ± 0.06 and 0.87 ± 0.02 for acetate-catalyzed hydrolyses of N-acetylbenzotriazole[27] and S-ethyl trifluorothioacetate,[28] respectively. (4) Diethyl p-nitrophenyl phosphate is a rapid irreversible inhibitor of EE-AChE-catalyzed hydrolyses of ATCh and BzCh, and BzCh is a mixed reversible inhibitor of EE-AChE-catalyzed hydrolysis of BzCh. Together these inhibitions suggest that the active site binding loci for ATCh and BzCh overlap. The carboxylate side chain of E199 is situated in the active site gorge of TC-AChE within 5 Å of the side chain oxygen of S200,[18] and thus provides a likely candidate for the general base catalyst of the slow substrate reactions.

Substrate activation is reported herein for the TC-AChE-catalyzed hydrolysis of BuTCh. This observation, like previous reports of substrate inhibition of AChE by ATCh[14] and ACh,[29] requires multiple sites on AChE for binding of quaternary ammonium ligands. The crystal structure of TC-AChE[18] supports this idea. The active site triad, S200–H440–E327, lies at the bottom of a 20-Å-deep gorge. In addition to E327, there are three carboxylate residues in the active site gorge: E199 is near the bottom of the gorge and is ~15 Å from the surface of the enzyme, D72 is ~10 Å up the gorge toward the surface, and E73 is just at the gorge opening. Moreover, there are numerous aspartate and glutamate residues on the face of the enzyme around the gorge opening. It is conceivable then that ATCh, BuTCh, and other choline substrates first encounter the enzyme surface distal to the active site and that diffusion on the surface is a component of the catalytic mechanism of AChE.

(25) Segel, I. H. *Enzyme Kinetics*; John Wiley & Sons: New York, 1975; pp 108–109.

(26) Kresge, A. J.; More O'Ferrall, R. A.; Powell, M. F. In *Isotopes in Organic Chemistry*; Buncel, E., Lee, C. C., Eds.; Elsevier: Amsterdam, 1987; Vol. 7, Chapter 4, pp 177–274.

(27) The Z value for acetate-catalyzed hydrolysis of N-acetylbenzotriazole was calculated by fitting proton inventory data from the following reference to eq 8: Gopalakrishnan, G.; Hogg, J. L. *J. Org. Chem.* **1981**, *46*, 4959–4964.

(28) Professor K. S. Venkatasubban kindly provided unpublished proton inventory data for acetate-catalyzed hydrolysis of S-ethyl trifluorothioacetate, which were analyzed according to eq 8 to give the cited Z value.

(29) Wilson, I. B.; Cabib, E. *J. Am. Chem. Soc.* **1956**, *78*, 202–207.

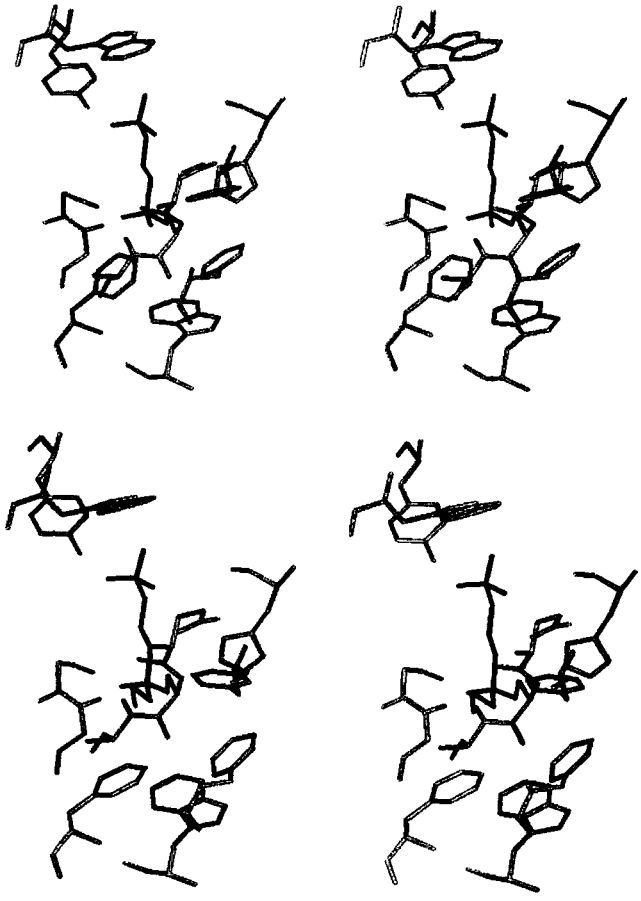

Figure 5. (top) Relaxed stereoview of the tetrahedral intermediate in the acylation stage of TC-AChE-catalyzed hydrolysis of ATCh. The substrate-derived portion of the complex is dark-shaded, with the quaternary amino function at the top and the acyl function, covalently attached to S200, at the bottom. The displayed amino acid side chains are, beginning at the top and proceeding clockwise, W84, E199, H440, F331, F288, W233, F290, and Y130. The oxyanionic O^- is within H-bonding distance of the peptide NH functions of G118 (2.6 Å), G119 (2.5 Å), and A201 (3.3 Å); these residues form the oxyanion hole[18] and are dark-tipped in the stereoview. Residues that make close contacts (i.e. 3–4 Å) with the acyl methyl function of ATCh are W233, F288, F290, F331, and H440. These residues comprise the acyl-binding pocket. (bottom) Relaxed stereoview of the tetrahedral intermediate in the acylation stage of TC-AChE-catalyzed hydrolysis of BuTCh.

Molecular modeling provides a rationale for the change in mechanism expressed by AChE when the acyl function of the substrate is larger than propanoyl. Figure 5 (top) shows a stereoview of the tetrahedral intermediate in the acylation stage of TC-AChE-catalyzed hydrolysis of ATCh. This model is similar to that described by Sussman *et al.*[18] for interaction of the enzyme with ACh and illustrates interactions between the substrate and functionalities in the active site gorge that are likely important for catalysis. The quaternary ammonio function makes close contacts (~3 Å) with W84, E199, and Y130. The anionic oxygen of the erstwhile substrate carbonyl points toward the peptide NH functions of G118, G119, and A201, the putative 'oxyanion hole'.[18] Of particular importance for the studies reported herein, the acetyl methyl function of the substrate is nestled in an acyl-binding pocket that is formed by the side chains of W233, F288, F290, F331, and H440.[30] In the model for the tetrahedral intermediate in BuTCh hydrolysis of Figure 5 (bottom), the butanoyl function adopts a conformation in which the C_α–Et function is *gauche* to the C–O^- and C–S bonds of the erstwhile carbonyl carbon, which points C_β away from the acyl-binding pocket. In addition, C_α and the residues of the acyl-binding pocket have moved away from each other by 0.2–0.3 Å when compared to the interactions in the ATCh model of Figure 5 (top). It is obvious that steric clashes with the acyl pocket tend to exclude the butanoyl function of BuTCh. Consequently, when the substrate acyl function is large (butanoyl or benzoyl) alternate binding modes in the active site gorge compete with that which leads to the tetrahedral intermediate in Figure 5 (bottom), and an alternate channel for catalysis is exposed.

AChE effects a large catalytic acceleration even when the cryptic mechanism is being utilized. As described earlier, EE-AChE-catalyzed hydrolysis of BzCh is 3.5×10^7 times faster than HO^- catalysis at the same pH. It is thus tempting to speculate that the cryptic mechanism is a vestige of a bygone era in the evolution of AChE catalytic power.

Acknowledgment. We thank Professor Israel Silman of the Weizmann Institute, Rehovot, Israel, for the kind gift of *Torpedo californica* AChE, and his co-worker, Lilly Toker, for skillful preparation of the enzyme. D.M.Q. thanks Dr. Erjdan Salih for interesting discussions of the various active protonic states of AChE. Molecular modeling was performed at the University of Iowa Image Analysis Facility. Support of this work was received from NIH Grant NS21334.

(30) Site-directed mutagenesis experiments support that F288 and F290 are components of the acyl-binding site. See ref 14c and the following: Harel, M.; Sussman, J. L.; Krejci, E.; Bon, S.; Chanal, P.; Massoulie, J.; Silman, I. *Proc. Natl. Acad. Sci. U.S.A.* **1992**, *89*, 10827–10831.